Weakly Coupled Relaxor Construction in Lead-free Ferroelectrics with Simple Composition for Superior Energy-Storage Performance

Minghao Liu[1,2], Chen Ming[3], Zhen Liu[1,], Hongbo Liu[2,*], Bing Han[1], Narendirakumar Narayanan[4], Xuantong Liu[5], Kai Dai[6], Teng Lu[5], Xuefeng Chen[1], Zhigao Hu[6], Yun Liu[5], Genshui Wang[1,3,7*]*

1, Key Laboratory of Inorganic Functional Materials and Devices, Shanghai Institute of Ceramics, Chinese Academy of Sciences, Shanghai 200050, China.

2, School of Materials Science and Engineering, Shanghai University of Engineering Science, Shanghai 201620, China.

3, State Key Laboratory of High Performance Ceramics and Superfine Microstructures, Shanghai Institute of Ceramics, Chinese Academy of Sciences, Shanghai 200050, China.

4, University of Missouri Research Reactor (MURR), University of Missouri, Columbia, Missouri 65211, USA

5, Research School of Chemistry, The Australian National University, Canberra, ACT 2601, Australia.

6, Technical Center for Multifunctional Magneto-Optical Spectroscopy (Shanghai), Engineering Research Center of Nanophotonics & Advanced Instrument (Ministry of Education), Department of Materials, School of Physics and Electronic Science, East China Normal University, Shanghai 200241, China.

7, School of Chemistry and Materials Science, Hangzhou Institute for Advanced Study, University of Chinese Academy of Sciences, Hangzhou 310024, China.

*Corresponding author: zhenliu@mail.sic.ac.cn, bohongliu@gmail.com, genshuiwang@mail.sic.ac.cn.

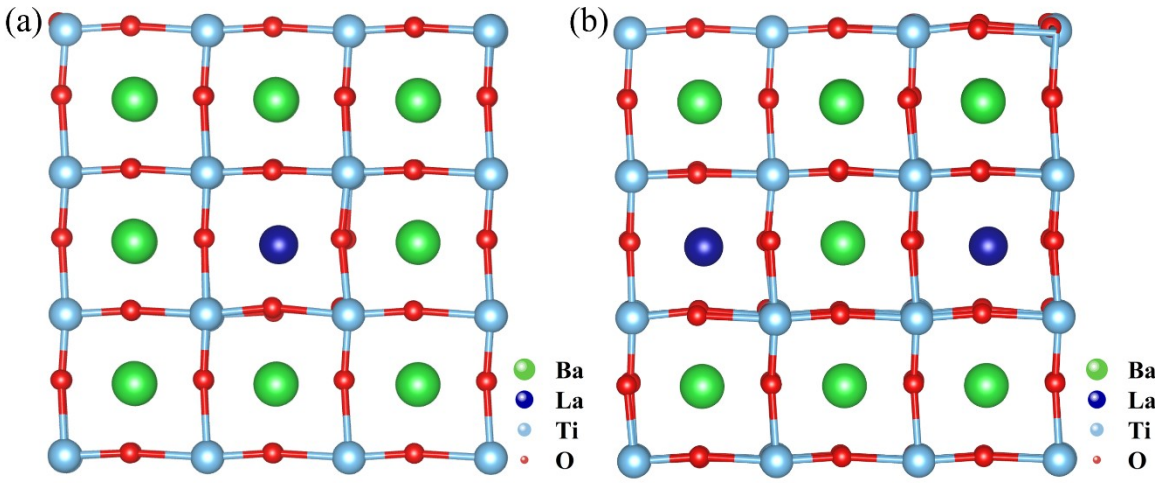

Figure S1. The supercell model of a) $(Ba_{23}La_1)Ti_{24}O_{72}$ and b) $(Ba_{22}La_2)Ti_{24}O_{72}$.

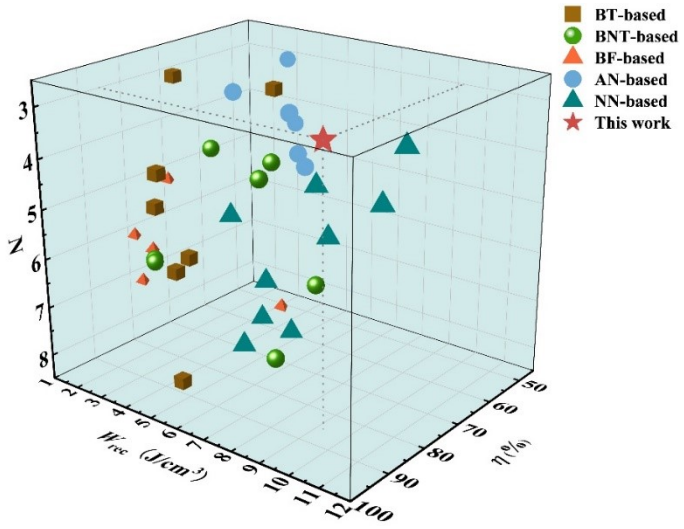

Figure S2. The comparison of energy storage parameters and corresponding number of elements excluding oxygen (N) for recently reported lead-free bulk ceramics.

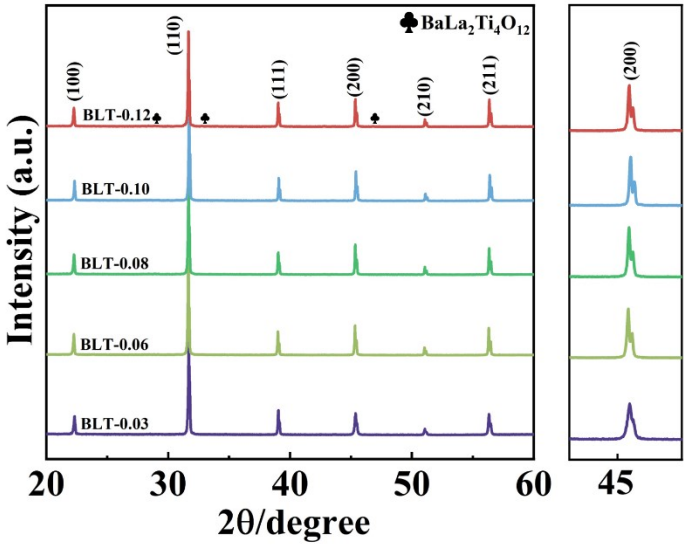

Figure S3. XRD patterns of the BLT-*x* ceramics at room temperature and the enlarged views of (002) peak.

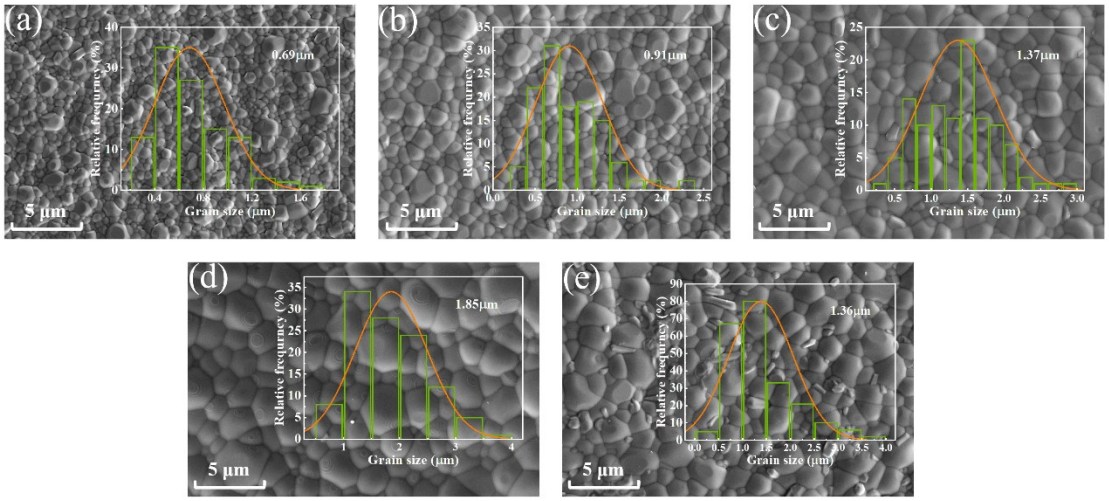

Figure S4. SEM pictures and grain size distributions of the a) BLT-0.03, b) BLT-0.06, c) BLT-0.08, d) BLT-0.1, and e) BLT-0.12 ceramics.

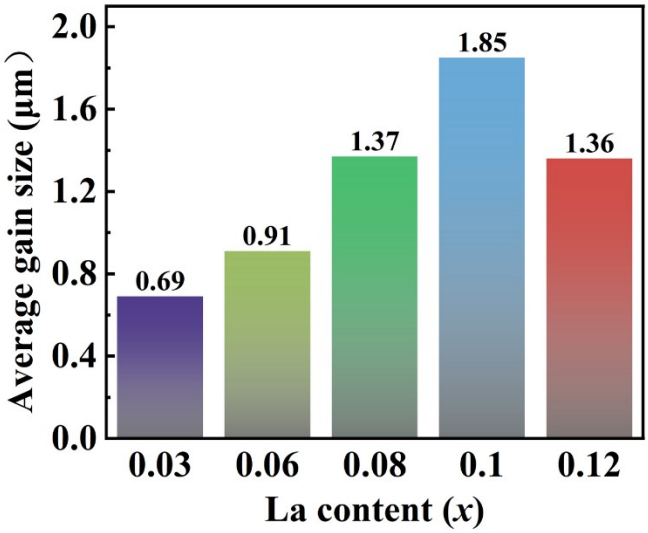

Figure S5. The average grain sizes of BLT-*x* ceramics.

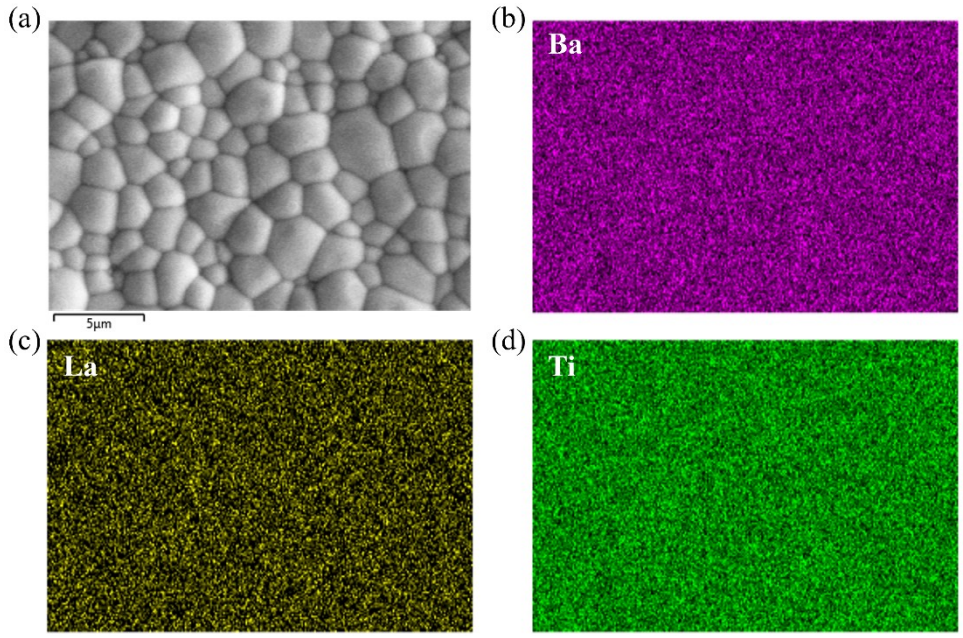

Figure S6. a) SEM surface morphology of BLT-0.12 ceramics. The element mapping of b) Ba, c) Ti, and d) La.

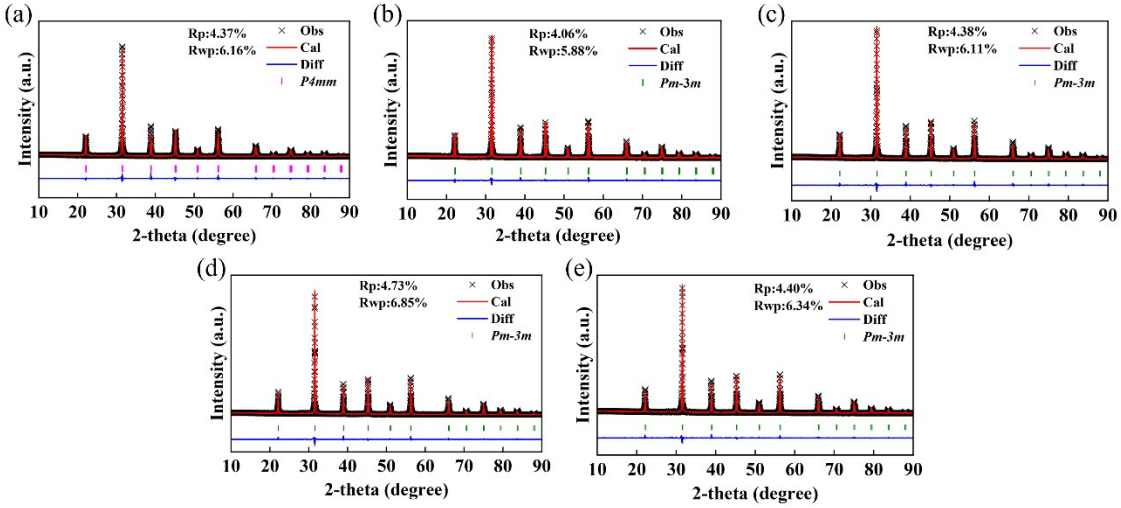

Figure S7. Rietveld refinement of XRD for a) BLT-0.03, b) BLT-0.06, c) BLT-0.08, d) BLT-0.10 and 4) BTAN-0.12 ceramics.

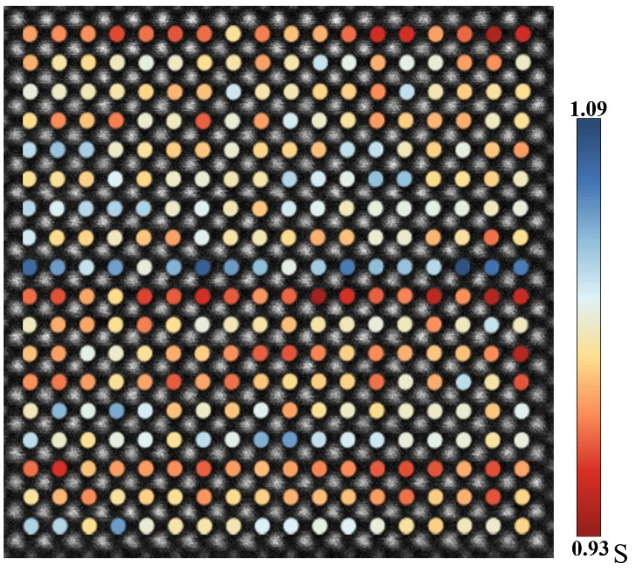

Figure S8. The represent unit cell c/a ratios of A-sites cations of BLT-0.10 ceramics along [100].

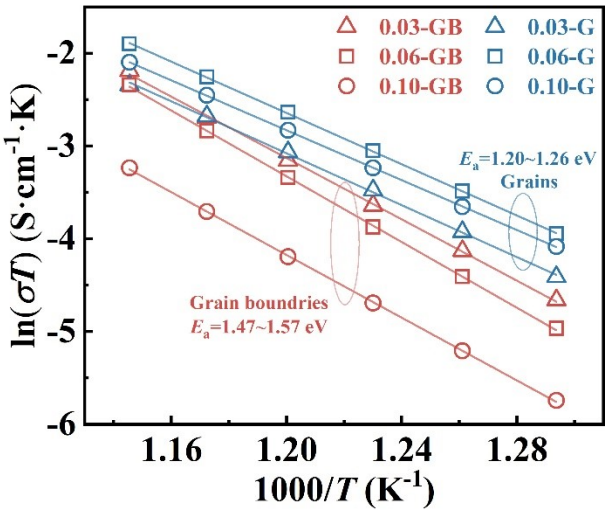

Figure S9. Arrhenius plots of total electrical conductivity and vacancy activation energy (E_a) for BLT-0.03, 0.08 and 0.10 ceramics.

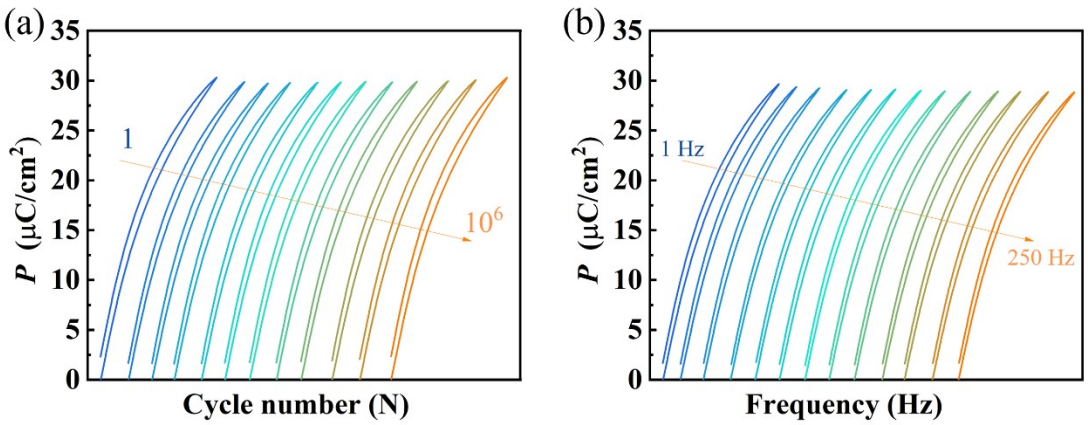

Figure S10. *P–E* loops of BLT-0.10 ceramics at different a) cycle numbers and b) frequencies.

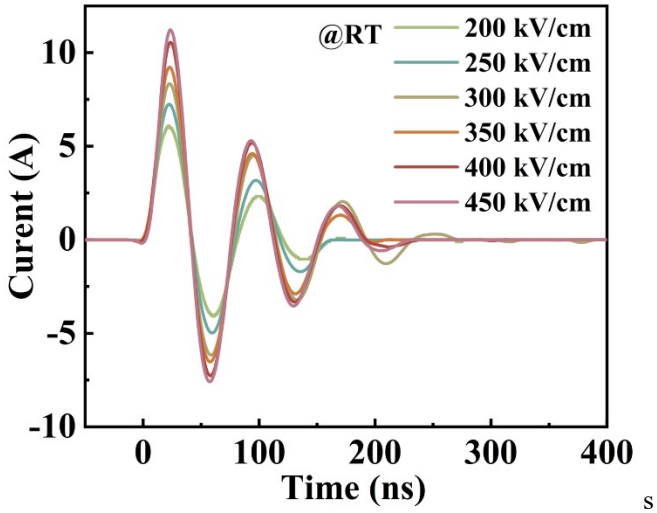

s

Figure S11. The underdamped charge-discharge curves of BLT-0.10 ceramics at 200-450 kV/cm.

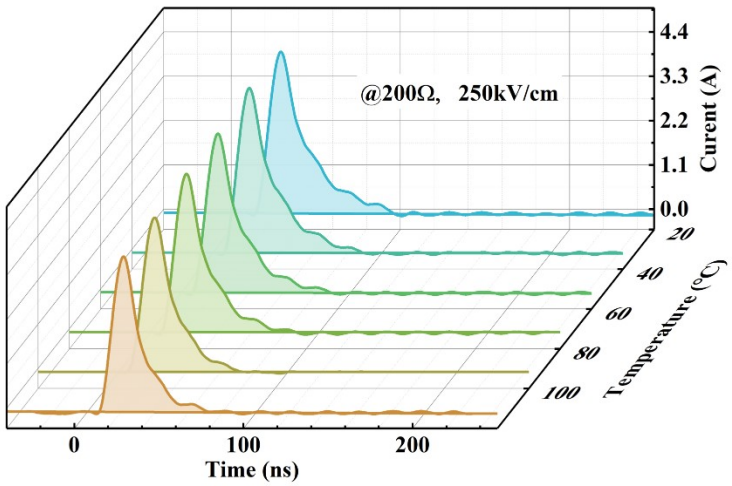

Figure S12. The overdamped charge-discharge curves of BLT-0.10 ceramics as a function of temperature.